

# Formation and evolution of shear structures in sheared granular gouge

Zhuan Dai<sup>1,2</sup>, Ke Gao<sup>1,3</sup> and Junlong Shang<sup>2,4</sup>

<sup>1</sup>Department of Earth and Space Sciences, Southern University of Science and Technology, 518055, Shenzhen, Guangdong, China  
E-mail: [gaok@sustech.edu.cn](mailto:gaok@sustech.edu.cn)

<sup>2</sup>James Watt School of Engineering, University of Glasgow, G128QQ, Glasgow, UK

<sup>3</sup>Guangdong Provincial Key Laboratory of Geophysical High-resolution Imaging Technology, Southern University of Science and Technology, 518055, Shenzhen, Guangdong, China

<sup>4</sup>Faculty of Science and Engineering, The University of Manchester, M139PL, Manchester, UK

Accepted 2025 May 7. Received 2025 April 10; in original form 2025 January 3

## SUMMARY

Fault cores have layered shear structures that evolve with time. Probing details of the accompanied gouge grain breakage and granular flow can unveil the complex evolving mechanism of fault. Here, irregular breakable grains are incorporated in a numerically simulated sheared granular gouge to show the evolution of shear structures. Granular quantities (e.g. non-affine displacement and local granular temperature) are adopted to depict the microstates of gouge in different macro shear stages and during stick-slips. Granular plasticity (defined as plastic granular flow here) is scattered in the linear stage, while it starts to cluster near the plate in the yield stage. Then, the shear localization becomes the strongest in the unstable shearing stage and weakens in the later stick-slip stage. In the stick phase during the stick-slip stage, some particles are more prone to unlocking due to the geometry of the fault and the arrangement of particles. Small local slips occur between these particles. The accumulation of small local slips between these particles can cause large dynamic failures. Finer grains in the principal slip zone decrease the transmitted shear force and render it easier for the granular gouges to rearrange themselves, causing the shear to localize in these zones. The long-term stick-slip cycles of natural faults result in the layered shear structures in the fault cores. Although the granular gouge between fault planes is composed of discrete particles or grains, the granular mass ruptures like a solid when slip events happen.

**Key words:** Fracture and flow; Numerical modelling; Crustal structure; Fractures, faults, and high strain deformation zones.

## 1 INTRODUCTION

Tectonic plates shear and grind with their counterparts, producing stick-slip cycles, and this stick-slip behaviour of faults is deemed an important mechanism of tectonic earthquakes (Byerlee & Brace 1968). Due to the pulverization of rocks, tectonic plates interact with each other through the granular gouge between fault planes (Ben-Zion & Sammis 2009). It is undeniable that the gouge plays a key role in stick-slips. Therefore, laboratory-scale sheared faults incorporating granular gouge are commonly employed to study tectonic earthquakes in controllable conditions (Marone 1998). Apart from the environmental conditions (e.g. normal pressure, shear velocity, temperature), researchers also focus on how the microscopic mechanism in gouge influences the macroscopic properties of faults (Ikari *et al.* 2015; Aubry *et al.* 2018; Passelegue *et al.* 2019).

In both laboratory earthquakes and natural faults, the shear structures in the fault core are not in a constant state but evolve with shear

(Scuderi *et al.* 2017; Okubo *et al.* 2019). The unique structures in natural fault cores may take thousands of years to form. Laboratory earthquakes present a similar process in a much shorter time, which may help us better understand the formation of structures in fault cores. Typical shear structures in laboratory earthquakes are shown in Fig. 1. Researchers found that a more continuous shear structure at long shear displacement can transform the fault from velocity-strengthening to velocity-weakening behaviour (Scuderi *et al.* 2017). Under different environmental conditions (e.g. different normal stresses), the faults show different slip modes, and the shear structures also have different evolution patterns (Pozzi *et al.* 2022; Pozzi *et al.* 2023). The shear structures are strongly correlated with the macroscopic properties of faults, and knowing the details of the formation and evolution of shear structures can help unveil the complex shearing process of natural faults.

Numerical simulation of laboratory fault gouges can provide more microscopic details that cannot be easily monitored using

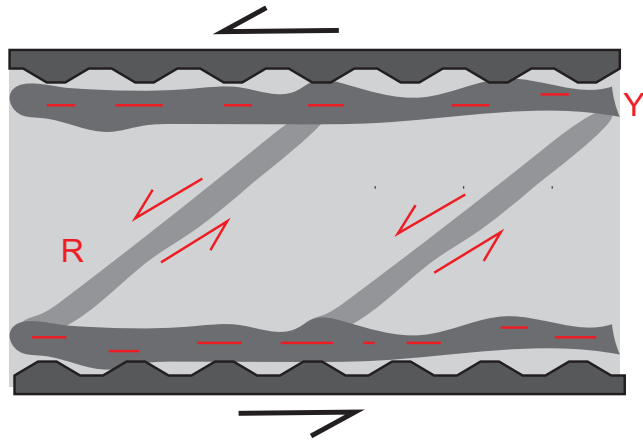


**Figure 1.** Typical shear structures in gouge (Mair & Marone 1999; Davis *et al.* 2000; Katz *et al.* 2004; Scuderi *et al.* 2017; Kimura *et al.* 2022; Pozzi *et al.* 2022). Y shear parallel with the shear direction. The angle between R shear and the shear direction is acute (usually about  $20^\circ$ ).

laboratory physical equipment, and it is thus a powerful supplementary tool for revealing micro granular flow in the gouge (Ferdowsi *et al.* 2014). The discrete element method (DEM) is capable of simulating discontinuous granular materials and is also widely used in the numerical simulation of sheared granular gouges (Mora & Place 1999; Morgan 1999; Place & Mora 2000; Munjiza 2004; Yu 2004). Generally, because we focus on the microscopic mechanism in gouge, the plates are simplified as rigid blocks in the numerical model. The normal stress and the load stiffness are adjusted to ensure the model can produce regular stick-slip cycles (Leeman *et al.* 2016; Dorostkar *et al.* 2017). With the detailed data of kinematics of gouge particles, granular physics quantities can be calculated, such as non-affine displacement (Chikkadi & Schall 2012), granular temperature (Zou *et al.* 2021), slipping contact ratio (Ferdowsi *et al.* 2013), and topology of Delaunay tessellation (Cao *et al.* 2018), to depict the microscopic characteristics in gouge. The micro property of gouge particles, which is hard to measure in the laboratory, can also be changed for a more systematic exploration. Casas *et al.* (2022) sheared a granular gouge with different percentages of particle cementation and explored how the cementation between particles influences the macro peak stress and the evolution of shear structures inside the gouge. Numerical simulations provide effective ways to connect the macroscopic properties of faults and their corresponding microscopic evolutions in gouge (Chikkadi & Schall 2012; Ferdowsi *et al.* 2013; Cao 2018).

To study the detailed evolution of shear structures and the effects caused by grain breakage, instead of purely adopting rigid gouge particles, researchers also constructed breakable grains in their numerical granular gouge. Some researchers used large breakable spherical gouge grains in their numerical simulations, each grain consisting of up to hundreds of gouge particles connected by breakable bonds (Abe & Mair 2005, 2009; Mair & Abe 2008; Ioannidi *et al.* 2024). This kind of model is suitable for showing how the grain size evolves during shearing. Guo & Morgan (2006) constructed rounded and triangular grains by connecting circular particles with breakable bonds to explore how the shape of grains influences the frictional behaviour of granular faults. Guo & Morgan (2007) also adopted breakable bulks to shear with each other to demonstrate how the gouge zone develops. However, relatively large irregular grains are observed in the real granular gouge (Sammis

*et al.* 1987; Billi 2005), and a full simulation process incorporating large irregular breakable grains under shear may tell us more microscopic process about the breakage of large irregular grains and evolution of accompanied shear localization. Relevant studies are still missing. The microscopic process can help explain the background mechanisms of some phenomena (e.g. fault lubrication, effects of the grain breakage) in natural faults and deepen our understanding of natural earthquakes (Di Toro *et al.* 2011), which may also shed light on the formation of shear structures inside gouges.

Aiming at studying the breakage effects of the large irregular gouge grains, here, a new sheared granular gouge model setup that incorporates large irregular breakable grains and sheared with finite stiffness is proposed. In our numerically simulated sheared granular gouge using DEM, rigid discs are bonded to form breakable grains of irregular shapes. Granular quantities (e.g. non-affine displacement and local granular temperature) are adopted to depict the microstates in the granular gouge. First, we construct a granular fault model (Section 2). The simulated fault is sheared through different macro stages. Then, based on the recorded microscopic information in the granular gouge, non-affine displacement is calculated to depict the plasticity in different macro stages, and the local granular temperature is calculated to depict the granular dynamics during stick-slips (Section 3). Finally, to further discuss the role of grain breakage in the shearing process, two extreme cases—one without bonds and one with unbreakable bonds—are compared (Section 4). We explain how shear structures form and evolve in the granular gouge. Conclusions are given at the end (Section 5).

## 2 METHODS

### 2.1 Model setup

This study conducts numerical simulations in PFC (Particle Flow Code, a DEM software) (Itasca 2021), which can simulate the motion and interaction of finite-size particles. In PFC, particles are rigid bodies with finite mass that move independently of each other and can be translated or rotated. The internal forces and moments generated by particles through contact interact with their neighbours, and the internal forces and moments between particles are calculated and updated through contact mechanics. The kinematic data of particles are obtained by explicitly solving Newton's motion equations in the DEM framework. PFC is suitable for simulating granular materials with discrete properties and, therefore, can be used for simulating sheared fault systems containing granular gouges.

Here, numerically simulated faults that incorporate breakable grains are constructed (Fig. 2), and the model setup mainly refers to the laboratory experiments of sheared gouge carried out by Scuderi *et al.* (2017) and Pozzi *et al.* (2022). We adopt rigid plates with finite roughness to facilitate the shear. Each plate consists of eight rigid discs with radii of  $250\ \mu\text{m}$  to ensure the shear force is applied to the gouge. Equivalent normal stresses (20 MPa) are applied on the top and bottom plates. The load point moves horizontally at a constant speed ( $0.1\ \text{m s}^{-1}$ ). It is worth noting that the shear velocity used here is much faster than that used in the laboratory experiments. This is purely for computational efficiency consideration. However, we make sure the granular gouge is in a dense regime and the normalized distribution of granular motion is similar (Li *et al.* 2024) (see the last part of this section). Then, the shear force

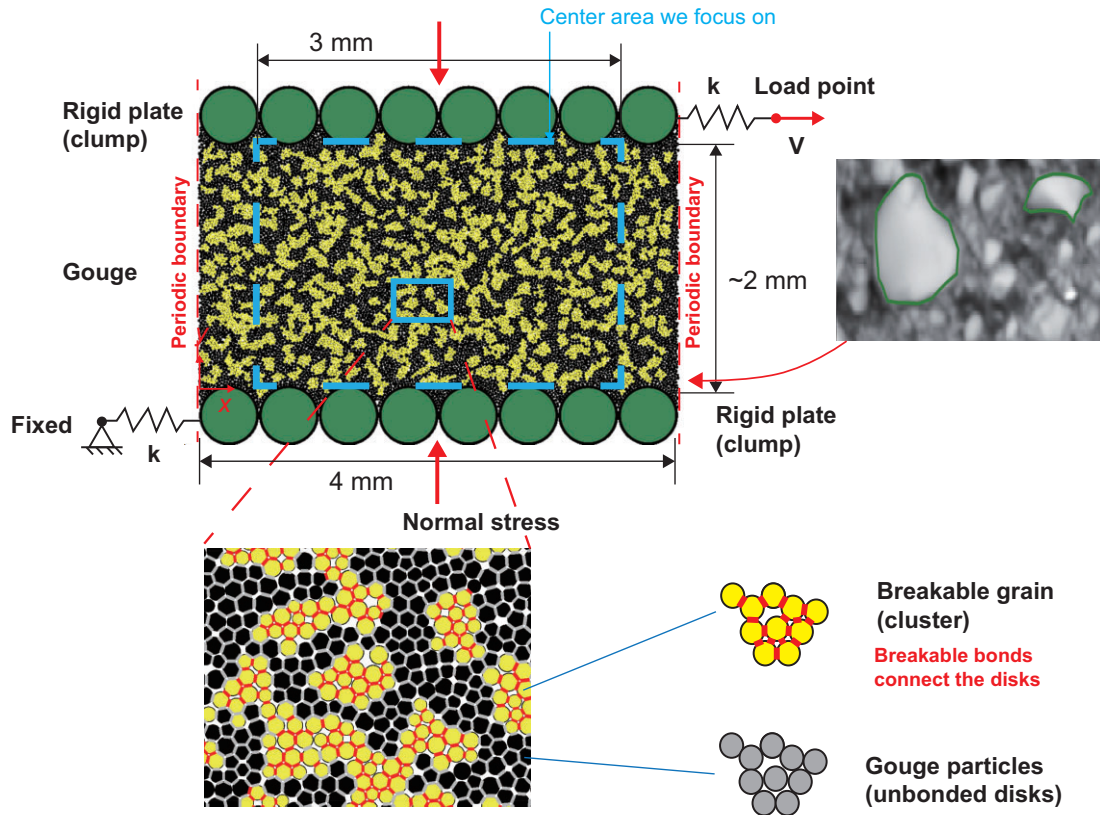


**Figure 2.** Numerical model of the sheared granular gouge with irregular breakable grains. The width of the model is 4 mm, and the thickness of the gouge is about 2 mm. To avoid the influence of period boundaries, the granular quantities are only calculated in the centre area (dashed rectangle). The 2-D geometries of quartz minerals grains are extracted from images of a quartz gouge and imported into PFC to construct a more authentic model.

is transmitted to the plate through an elastic spring, thereby applying shear stress to the top plate. At the same time, a fixed point is connected to the bottom plate with an elastic spring. The stiffness of both springs is  $1.232 \times 10^8 \text{ N m}^{-1}$  (estimated from the slope of the force-displacement curve in the liner stage in the experiments of Scuderi *et al.* (2017) and Pozzi *et al.* (2022)). To achieve a large shear strain in the model, periodic boundary conditions are applied at both ends of the model. Further analysis of microdynamics focuses on the central area with a 3 mm width to avoid the possible influence of periodic boundaries (indicated by the cyan dashed rectangle in Fig. 2).

The 2 mm-thick granular gouge consists of 11 468 rigid disc particles (radius 10–15  $\mu\text{m}$ ). Some (~39 per cent, estimated from the quartz gouge image) are bonded through breakable bonds to construct irregular breakable grains. It is worth noting that ‘grain’ refers to bonded particles hereafter. These bonds can capture the tension and shear forces within particles before the contact failure. The bonds will be removed when they fail, and then the particles involved can move freely. Other fault gouge particles are unbonded discs and can only sustain normal and friction forces due to interactions with their neighbours. The Linear Parallel Bond Model (Potyondy & Cundall 2004; Holt *et al.* 2005) and Linear Model (Cundall & Strack 1979) are respectively used for solving the mechanics states for bonded and unbonded particles. After the failure of a bond, the Linear Parallel Bond Model degrades to the Linear Model. More details about the two models are introduced in the supplement material (Text S1). We calibrate the microcontact parameters to compute the contact force through a

test and error process (Text S2). The macro properties of breakable grains here resemble strong minerals like quartz (Villeneuve *et al.* 2012). The density, friction coefficient, Young’s modulus, Poisson’s ratio, tensile strength and uniaxial compression strength are  $2650 \text{ kg m}^{-3}$ , 0.65, 67.4 GPa, 0.08, 63.17 MPa and 200.16 MPa, respectively. Microscopic parameters and other details are listed in Table S1.

To construct a more authentic model, we extract 400 grain boundaries from images of a quartz gouge from the work of Scuderi *et al.* (2017). Then, we generate breakable grains as follows (see workflow in Fig. 3). (1) Import the geometry of a random grain. (2) Calculate its effective diameter and centroid. (3) Scale its geometry to a random effective diameter (40–60  $\mu\text{m}$ ). (4) Rotate and translate the geometry to a random position. (5) Check if the random position is appropriate; specifically, a grain overlaps with the formerly generated grains or the nodes of the grain outside the model are considered as inappropriate. If this occurs, move back to step (4). (6) If the random position is appropriate, bond the discs inside the geometry. Loop steps (1)–(6) until the fraction of bonded grains reaches the target value (~39 per cent).

The simulation involves the following steps, that is, sample preparation, consolidation and shearing. For sample preparation, first, the space between the plates is filled with rigid discs (radius of 10–15  $\mu\text{m}$ ). This step is done by randomly generating overlapping discs. In the meantime, a small stiffness is assigned to the discs so they interact with each other and gradually fill the space. We ensure the number of discs is not too large to result in stress heterogeneity and not too small so that the discs are well in contact with their

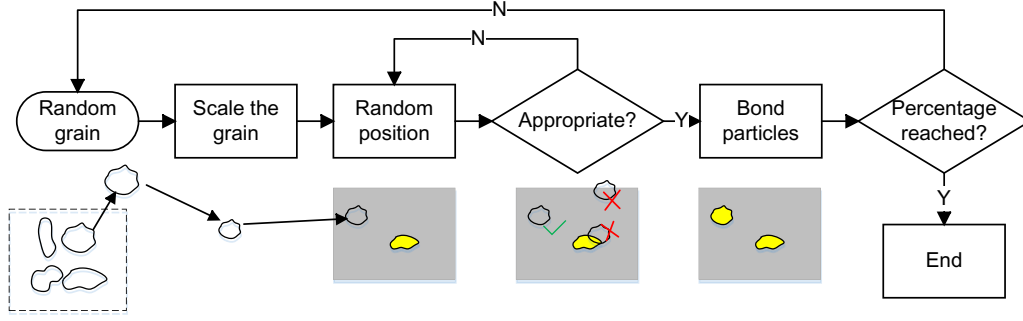


**Figure 3.** Workflow to construct irregular breakable grains with the aid of real gouge particle image. ‘N’ denotes ‘No’ and ‘Y’ denotes ‘Yes’.

neighbours. Then, we generate irregular breakable grains using the method introduced in the previous paragraph, and the microcontact parameters we get from the test and error process are assigned to the discs and their contacts. After this, we gradually consolidate the gouge until the target normal stress (20 MPa) is reached (Text S3). The normal stress is added slowly so that the grains will not be crushed dynamically in the consolidation stage. Finally, we maintain the normal stress and shear the gouge with constant velocity at the load point. The inertial number (da Cruz *et al.* 2005; Fei *et al.* 2020) of the model is  $I = \dot{\gamma} d \sqrt{P/\rho} \approx 1.44 \times 10^{-8} < 10^{-3}$ , indicating that the system is in a quasi-static shearing state and the macroscopic deformation is much slower than the microscopic rearrangement, which guarantees the granular material is in a dense state, where  $\dot{\gamma}$  is the shear rate,  $d$  is the particle’s average diameter,  $P$  is normal pressure and  $\rho$  is the particle’s density. The  $\dot{\gamma}$  is calculated by

$$\dot{\gamma} = \frac{V}{H_m}, \quad (1)$$

where  $H_m$  is the height of the model ( $\sim 2$  mm) and  $V$  is the shear velocity applied on the load point.

## 2.2 Granular characteristics

To describe the behaviour of the discrete granular material, after obtaining detailed information about the motion of particles, their granular physical quantities can be calculated to further quantify the motion of particles and to establish a connection between the microscopic and macroscopic mechanical behaviour. In the shearing process, the topology of the granular gouge changed significantly, which means it is difficult to calculate the strain of the granular gouge in a traditional way. The displacement gradient is also an effective way to show the localization, but we must select a direction for calculating the gradient so the shear localization in other directions may be ignored. Here, to capture and quantify the plastic granular flow in the granular gouge and show the evolution of shear structures, we calculate the non-affine displacement (Ma *et al.* 2021) to demonstrate how the shear localization evolves in the granular gouge. To quantify the friction and collision of the particles and grains during stick-slip cycles, local granular temperature (Zou *et al.* 2021) is adopted to depict the microscopic dynamics in the granular gouge.

### 2.2.1 Granular plasticity

The plasticity in granular gouge can be depicted by the non-affine displacement (Ma *et al.* 2021). The non-affine displacement of a

particle is the deviation of the particle’s position from the best-fitting affine transformation over the shear strain window  $\Delta\gamma$ , that is,

$$D_{\min}^2(\gamma, \Delta\gamma) = \frac{1}{N_i} \sum_j^{N_i} |\mathbf{r}_j(\gamma + \Delta\gamma) - \mathbf{r}_i(\gamma + \Delta\gamma) - \mathbf{J}[\mathbf{r}_j(\gamma) - \mathbf{r}_i(\gamma)]|^2, \quad (2)$$

where  $\mathbf{r}_i(\gamma)$  represents the coordinate of particle  $i$  when the macroscopic shear strain is  $\gamma$ . The subscript  $i$  denotes the designated particle, and the index  $j$  iterates over its  $N_i$  neighbours within a cut-off distance  $w$  relative to the reference particle  $i$  at  $\mathbf{r}_i(\gamma)$ . Here,  $\gamma$  is the macroscopic shear strain of the system at time  $t$  and is defined as the ratio of the displacement at the load point to the thickness of the gouge, and  $\mathbf{J}$  is the best-fitting affine transformation tensor that minimizes the quantity  $D_{\min}^2$ .  $\mathbf{J}$  can be calculated using the following equations:

$$\mathbf{X} = \sum_j^{N_i} [\mathbf{r}_j(\gamma + \Delta\gamma) - \mathbf{r}_i(\gamma + \Delta\gamma)] \otimes [\mathbf{r}_j(\gamma) - \mathbf{r}_i(\gamma)], \quad (3)$$

$$\mathbf{Y} = \sum_j^{N_i} [\mathbf{r}_j(\gamma) - \mathbf{r}_i(\gamma)] \otimes [\mathbf{r}_j(\gamma) - \mathbf{r}_i(\gamma)], \quad (4)$$

and

$$\mathbf{J} = \mathbf{X} \cdot \mathbf{Y}^{-1}. \quad (5)$$

Here,  $D_{\min}^2(\gamma, \Delta\gamma)$  can be deemed as the accumulation of granular plastic flow in the gouge from  $\gamma$  to  $\gamma + \Delta\gamma$  which indicates the shear localization in the gouge (see in Fig. 4). To describe the general characteristic of the plastic granular flow,  $\Delta\gamma$  should be large enough (e.g. contain a full stick-slip cycle) to avoid reflecting local biased phenomenon and also small enough not to overpass the range of the corresponding macro stage.

Then, the correlation function (Zou *et al.* 2021; Mei *et al.* 2023) can be introduced to characterize the spatial distribution of granular plasticity (indicated by the non-affine displacement) in different states, that is,

$$C(\Delta r) = \frac{(\langle c(r + \Delta r)c(r) \rangle - \langle c(r) \rangle^2)}{(\langle c^2(r) \rangle - \langle c(r) \rangle^2)}, \quad (6)$$

which calculates the correlation of non-affine displacement at locations separated by mutual distance  $\Delta r$ . Here,  $c(r)$  is the non-affine displacement  $D_{\min}^2(\gamma, \Delta\gamma)$  of the particle at position  $r$ , and  $c(r + \Delta r)$  represents  $D_{\min}^2(\gamma, \Delta\gamma)$  of particles with mutual distances of  $\Delta r$  to the particle at position  $r$ . The correlation function  $C(\Delta r)$  can be a quantitative indicator for comparing the spatial distribution of granular plasticity of our simulated fault at different macro stages. A larger  $C(\Delta r)$  means that the  $D_{\min}^2(\gamma, \Delta\gamma)$  has more similar values

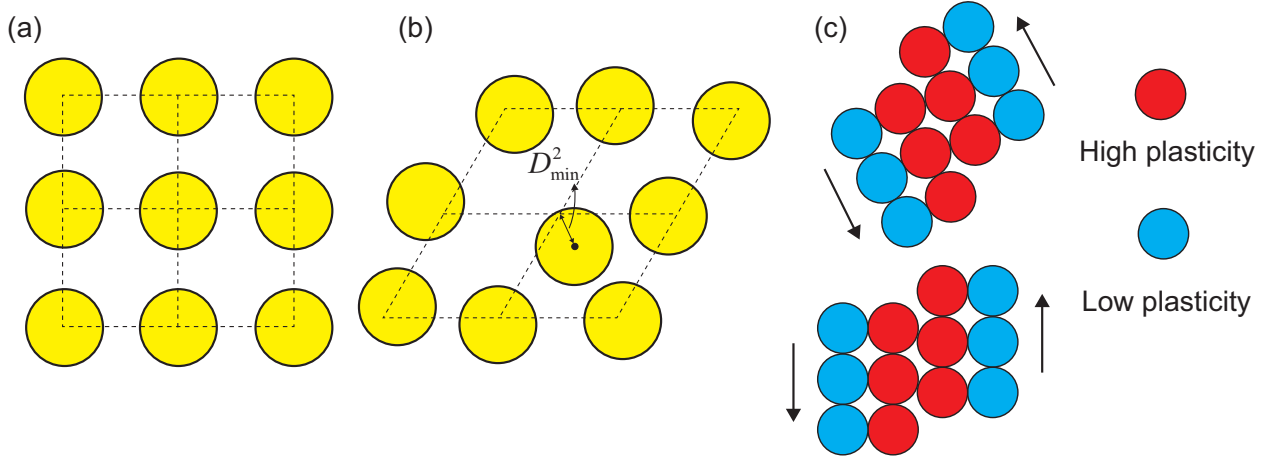


**Figure 4.** Illustration of the granular plasticity. (a) Assumed particle arrangement before shear and dashed lines show the overall shape of the granular mass. (b) Particle arrangement after disturbance and dashed lines show the overall shape [the overall shape in (a) after affine deformation]; the deviation of a particle's displacement from affine displacement is the non-affine displacement  $D_{\min}^2$  of the particle. (c) Particles with high granular plasticity show the plastic flow in the granular materials.

at the prescribed mutual distance  $\Delta r$ , which also means the correlation is stronger. Then, the correlation function  $C(\Delta r)$  is fitted by an exponential function  $C(\Delta r) \sim \exp(-\Delta r/\xi)$ , where  $\xi$  is the correlation length. A larger  $\xi$  represents the  $C(\Delta r)$  needs longer  $\Delta r$  to decay to a low value, which means that the  $D_{\min}^2(\gamma, \Delta\gamma)$  has a stronger long-range correlation.

### 2.2.2 Granular dynamics

We use the local granular temperature (Zou *et al.* 2021) to depict the microscopic dynamics in the gouge. The local granular temperature is defined as

$$T_{\text{loc}} = \frac{1}{3N_i} \sum_i^{N_i} |\mathbf{v}_i - \bar{\mathbf{v}}|^2, \quad (7)$$

where  $\mathbf{v}_i$  is the velocity of particle  $i$  and the index  $j$  iterates over its  $N_i$  neighbours and

$$\bar{\mathbf{v}} = \frac{\sum_j^{N_i} \mathbf{v}_j |\mathbf{v}_j|}{\sum_j^{N_i} |\mathbf{v}_j|}. \quad (8)$$

Two particles are deemed neighbours if their distance is within a cutoff distance of  $w$ . The local granular temperature quantifies the velocity difference between a particle and its neighbours and can be deemed as a measurement of local collision and friction of particles. The higher the local granular temperature, the more intense the collision and/or friction.

## 3 RESULTS

In this section, the general kinematics of the simulated faults at different macro stages are depicted by the macroscopic friction coefficient and the plate differential velocity. Then, we show how the granular plasticity evolves at different macro stages and how the granular dynamics develop during the stick-slip cycles.

### 3.1 General results

The general kinematics of the sheared fault are shown in Fig. 5. With the increase of load point displacement, the simulated fault

evolves in four stages: (I) linear stage, (II) yield stage, (III) unstable shearing stage and (IV) stick-slip stage. To depict the general kinematics of the simulated fault, the ratio between the shear and normal stress imposed on the gouge is defined as the macroscopic friction coefficient ( $\mu$ ), and the magnitude of the velocity difference between the top and bottom plate is defined as the plate differential velocity ( $|\Delta v_p|$ ). In the linear stage,  $\mu$  increases linearly (Fig. 5b), and the plates barely move relative to each other, so the  $|\Delta v_p|$  is nearly stabilized at 0 (Fig. 5d). In the yield stage, although  $\mu$  still increases, some small friction drop events occur (Fig. 5b). The plates move toward reverse directions with a relatively low velocity ( $|\Delta v_p| \sim 0.1 \text{ m s}^{-1}$ ) at these small friction drops (Fig. 5d). In the unstable shearing stage, the increasing trend of  $\mu$  disappears and large friction drops can be observed (Fig. 5b). The plates move toward reverse directions with large velocities ( $|\Delta v_p|$  up to  $\sim 4.8 \text{ m s}^{-1}$ ) at these large slip events (Fig. 5d). Finally, the unstable shearing evolves into a stick-slip stage, with a relatively smaller magnitude of friction drop (Fig. 5b) and shorter recurrence time of slip events than the unstable shearing stage (Fig. 5d). We also conduct two additional simulations with breakable grains (two newly constructed sheared granular faults), and they all show four similar stages (Fig. S2 and Fig. S3).

### 3.2 Granular plasticity

To characterize the plasticity in the sheared granular gouge in each of the four stages, the normalized non-affine displacements ( $D_{\min}^2 / \langle D_{\min}^2 \rangle$ ) in the four stages (marked in Fig. 5) are calculated (Fig. 6), which shows the accumulated plasticity in the four stages. These four stages undergo the same shear displacement long enough to contain several stick-slip cycles. Here, we focus on the spatial distribution pattern of granular plasticity so that the non-affine displacement is normalized by the average non-affine displacement at each stage. Granular plasticity quantifies the dislocation between a particle and its neighbours, and the layer it concentrates on reflects the shear localization in this layer.

In the linear stage (Figs 6a and e), the places with higher granular plasticity are scattered in the gouge because most particles and bonded grains are locked by their neighbours. The gouge shows little shear localization and manifests a linear increase in the macroscopic friction coefficient. However, in the yield stage (Figs 6b

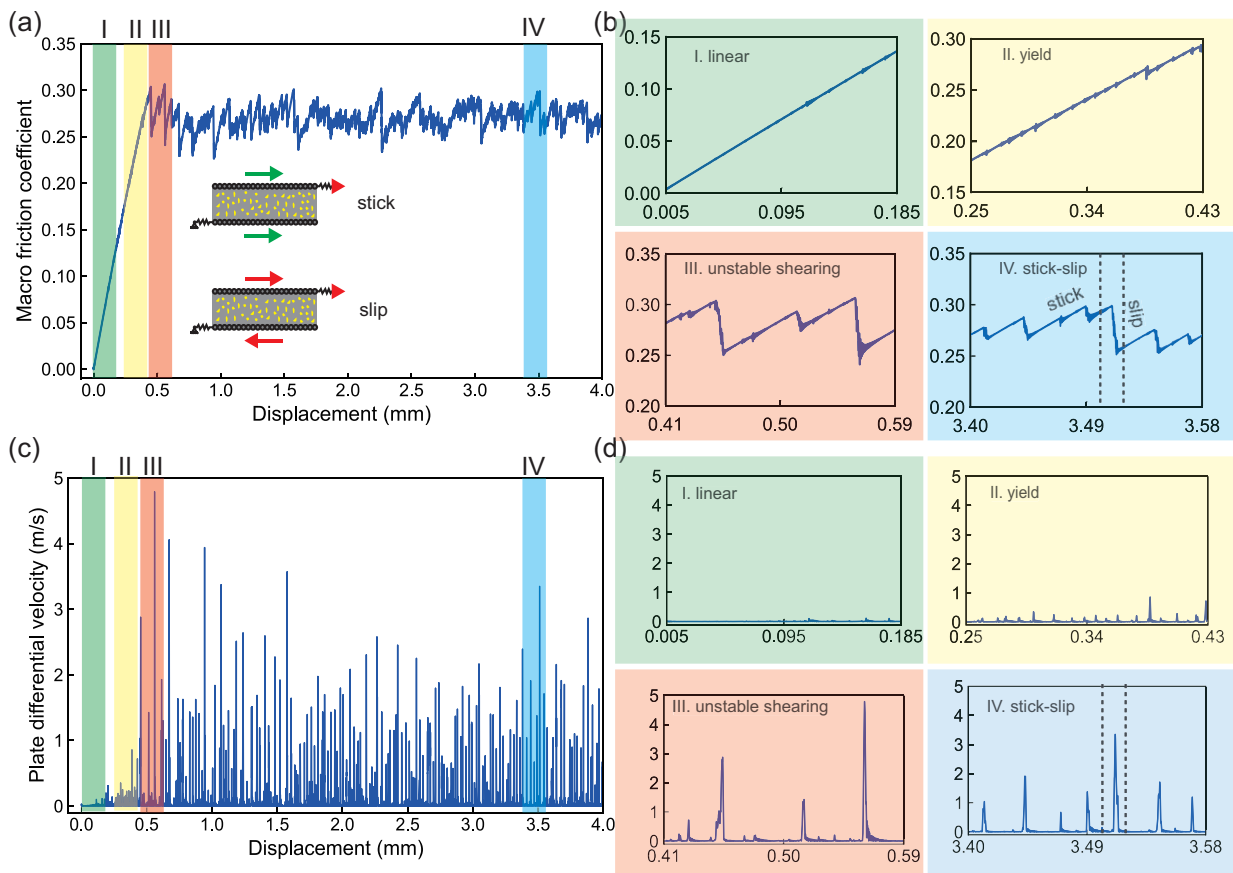


**Figure 5.** General results of the simulated sheared granular fault. (a) The evolution of the macroscopic friction coefficient with the load point displacement, and the inset shows the plate motion state in stick-slip. Four typical periods are marked by different colours, and these marked periods correspond to the linear stage, yield stage, unstable shearing stage and stick-slip stage, respectively. (b) Enlargement of the four typical periods. (c) Plate differential velocity versus the load point displacement. The same four typical periods in (a) are marked by different colours. (d) Enlargement of the four typical periods.

and f), the places with higher plasticity start clustering near the plate. In this stage, small slips start to occur, unlocking some particles and inducing the plate motion. Due to the released energy in each small slip, the particles near the plates are driven to flow plastically and shear localization can be observed (granular plasticity cluster to the two plates). Then, in the unstable shearing stage (Figs 6c and g), large slip events accompanied by strong shear localization in the gouge due to the dramatic release of elastic energy force the plates to crush the grains in the gouge (granular plasticity strongly localized near the load plate). However, at this stage, the localization of granular plasticity will decrease because more grains are crushed. Finally, the granular plasticity enters a stick-slip stage (Figs 6d and h), and the shear localization zone expands due to more grains being crushed (wider distribution zone of granular plasticity compared to before). The breakage of large grains renders the particles in the corresponding layer easier to flow and causes the plasticity to localize in this layer. The two additional numerical simulations presented in Fig. S4 and Fig. S5 also show similar characteristics.

Although the distribution pattern of granular plasticity in the four stages differs a lot, the probability density of  $D_{\min}^2 / \langle D_{\min}^2 \rangle$  in all states decreases logarithmically in a similar trend (Fig. 7a), which may be caused by the similar geometry of the sheared fault and gouge particles. The spatial distribution of the correlation of non-affine displacement varies (Fig. 7b). The linear stage has the weakest spatial correlation since the particles are locked and barely move

relative to each other. Then, small slips occur in the yield stage, and particles near the plate are easily driven by the plate, in which place the plasticity has a clustering trend, and thus with an increasing correlation. Catastrophic failure happens for the first time in the gouge in the unstable shearing stage. The unstable shearing stage has the strongest correlation because most grains are still intact and jam the gouge, so the plasticity localizes near the plates. However, with the breakage of the grain, more areas are unjammed; thus, the localization of the plasticity decreases, and so does the spatial correlation.

## 4 DISCUSSION

In this section, the formation of the shear structure in the gouge is explained from a granular motion viewpoint. Then, the effects caused by the breakage of grains are explored by analysing another two extreme cases. Finally, typical principal slip zones in laboratory earthquakes and their link to natural faults are discussed, and we also discussed the limitations of our numerical model.

### 4.1 From granular motion to shear structures

To unveil the micro-dynamics during stick-slips, we animate the normalized local granular temperatures ( $T_{loc} / \langle T_{loc} \rangle$ ) (Video S1), and the start and end of the selected stick-slip cycle in the stick-slip

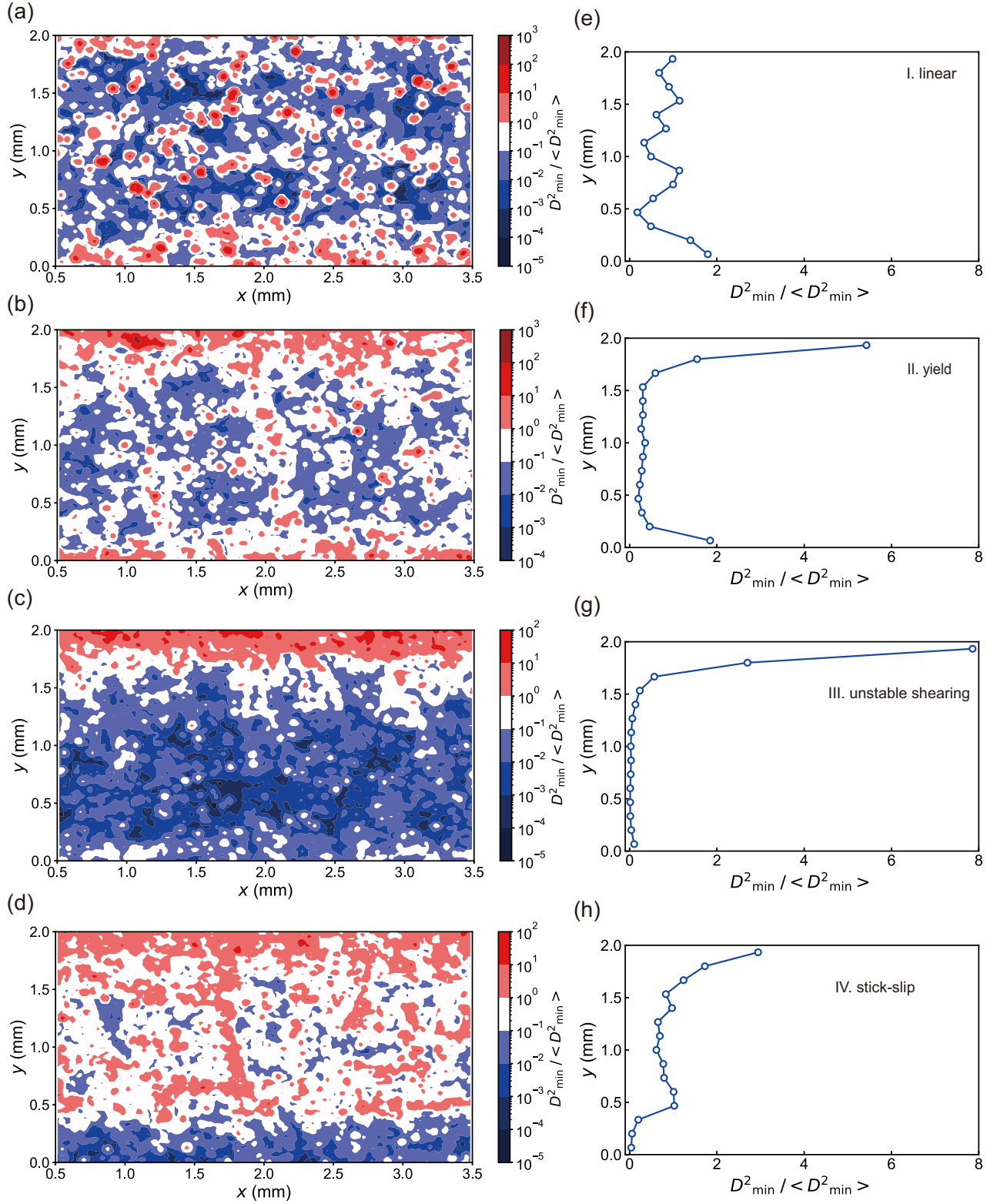


**Figure 6.** Granular plasticity in different stages. (a)–(d) are the cloud maps of non-affine displacement, and (e)–(h) are the corresponding average values of non-affine displacement along the  $y$ -axis. We use an arithmetic sequence to divide the  $y$ -axis into 15 equal layers and calculate the average  $D^2_{\min} / \langle D^2_{\min} \rangle$  of particle for each layer.

stage are marked in Figs 5(b) and (d) by the dashed lines. Places with extremely high  $T_{loc} / \langle T_{loc} \rangle$  (high-temperature areas) are scattered in the gouge, and they dramatically heat up when entering the slip

phase. According to the distribution and evolution of  $T_{loc} / \langle T_{loc} \rangle$ , we infer that small slips between particles exist in the stick phase, and these slips will be dramatically accelerated in the slip phase.

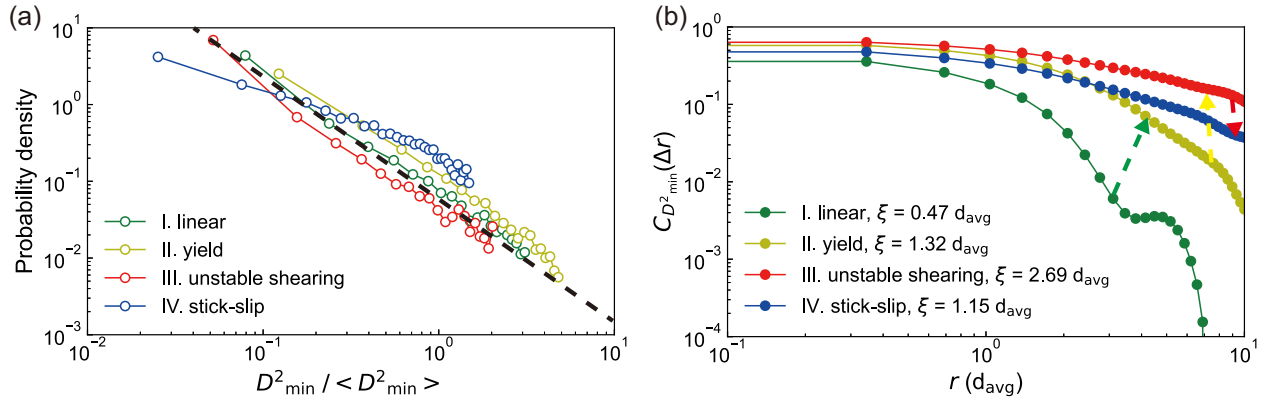


**Figure 7.** Distribution and the correlation of granular plasticity. (a) Distribution of the normalized non-affine displacement in the four shearing stages. The dashed black line indicates the universal trend for the four stages. (b) Correlation of non-affine displacement in the four shearing stages.

Although the granular material is composed of discrete particles and can flow like fluid when in the presence of external influences (Kou *et al.* 2017), during stick-slip cycles, the trigger of a slip event is similar to the failure process of brittle solid materials. In the stick phase, some particles are more prone to unlock due to the geometry of the fault or the arrangement of these particles (Fig. 8a). Therefore, small slips occur between these particles. These particles play a role similar to the microscopic cracks in solid materials, which can trigger catastrophic failures. The accumulation of small slips between these particles can cause dynamic failure around their locations (Fig. 8b). The produced small slips activate the gouge with a large slip event, and the plates move toward reverse directions and release the stored elastic energy dramatically (Fig. 8c). The inner failure in the granular gouge accelerates, forming the R shear. This can also accelerate the plates to frictionate fiercely with its counterpart, yielding the Y shear. After the slip, a new cycle starts (Fig. 8d).

The angle between the R shear and the fault plane can be explained by the Mohr–Coulomb criterion (Fig. 8e). The particles lock each other, forming a granular assembly in the stick phase. Its strength can be approximately described by the Mohr envelope, which means the stress states in the gouge should satisfy  $|\tau| \leq -\mu\sigma$ , where  $\mu$  is the friction coefficient between particles,  $\sigma$  and  $\tau$  are the normal stress and shear stress, respectively. After consolidation, the applied stress on the fault plane is  $\sigma_n$ , which is also the maximum principal stress at this state (green Mohr circle in Fig. 8e). As the shear goes, the Mohr circle is enlarged, and the corresponding position of the fault plane in the Mohr circle also evolves. When the Mohr circle touches the Mohr envelope, there will be two possible failure surfaces. One failure surface corresponds to a positive  $\tau$  (red dashed line in Fig. 8e), and the other corresponds to a negative  $\tau$  (cyan dashed line in Fig. 8e). The relative movement directions on the failure surface correspond to a positive  $\tau$ , which is more consistent with the shear load on the faults. Therefore, this kind of failure can easily occur and is then accelerated by the relative movement of the fault planes, yielding the R shears. To accommodate the relative displacement of the fault planes, the Y shears parallel to the faults are formed, and some of them join the formed shear structures, which constitute the principal slip zone after long shear displacement (Fig. 8f).

Here, due to the relatively stiff spring in the model, after each slip event, the differential plate displacement is small ( $\sim 10^{-2}$  mm). Therefore, in a slip event, we can see more scattered high granular temperature areas occur, and the fierce collision and friction of

particles only exist locally. Casas *et al.* (2022) found that with the increase of cementation between particles, more continuous R shears can be found in the granular gouge. Therefore, another reason there is no continuous R shear is that we shear dry gouge lacking cementation.

R shear and Y shear are the most basic and common shear structures. In real experiments or natural faults, when the geometry of the fault is more complicated or the compositions of granular fault cores are more heterogeneous, the shear structures may have a more random pattern. For example, the R' shear (cyan dashed line in Fig. 8e) can also occur. Additionally, because the accumulated shear strain in R shears also has shear effects on the parts between them, some subshear structures that conjugate with or link the parallel R shears can also be formed at large shear displacement (P shear and P' shear) (Bally 1983).

## 4.2 The effects of grain breakage

To illustrate the effect of grain breakage during the shear, we conduct two additional extreme cases: one without bonds (only rigid particles) and one with unbreakable bonds (bonds with infinite strength) (Fig. 9). The first several friction drops (0.2–0.5) of these two new models are much larger than the previous model (0.05) with breakable grains (Fig. 5), which indicates that without breakable bonds, the size of the initial friction drops will increase. This is because the continuing breakage of breakable bonds releases the energy gradually in advance. The small quakes caused by the breakage of weak bonds render the gouge layer a looser particle contact structure, resulting in smaller first several friction drops in the model with breakable bonds. Besides, the fault strength (macroscopic friction coefficient) of the model with unbreakable bonds is stronger, and the duration of the stick procedures is generally longer than that of the other two models (the previous model with relatively breakable bonds and the new model without bonds).

The distribution and spatial correlation of the granular plasticity in the two new models are shown in Fig. 10, and the corresponding results in the unstable shearing and stick-slip stages in the model with breakable grains are also plotted for comparison. The probability density of  $D_{\min}^2 / \langle D_{\min}^2 \rangle$  in all models decreases logarithmically in a similar trend (Fig. 10a). However, the correlation in the model without bonds is the strongest (Fig. 10b). Without bonded grains, the granular gouge can flow more easily and thus result in stronger shear localization compared to the model with unbreakable bonds (Figs 9a and c). Conversely, for the model with unbreakable grains,

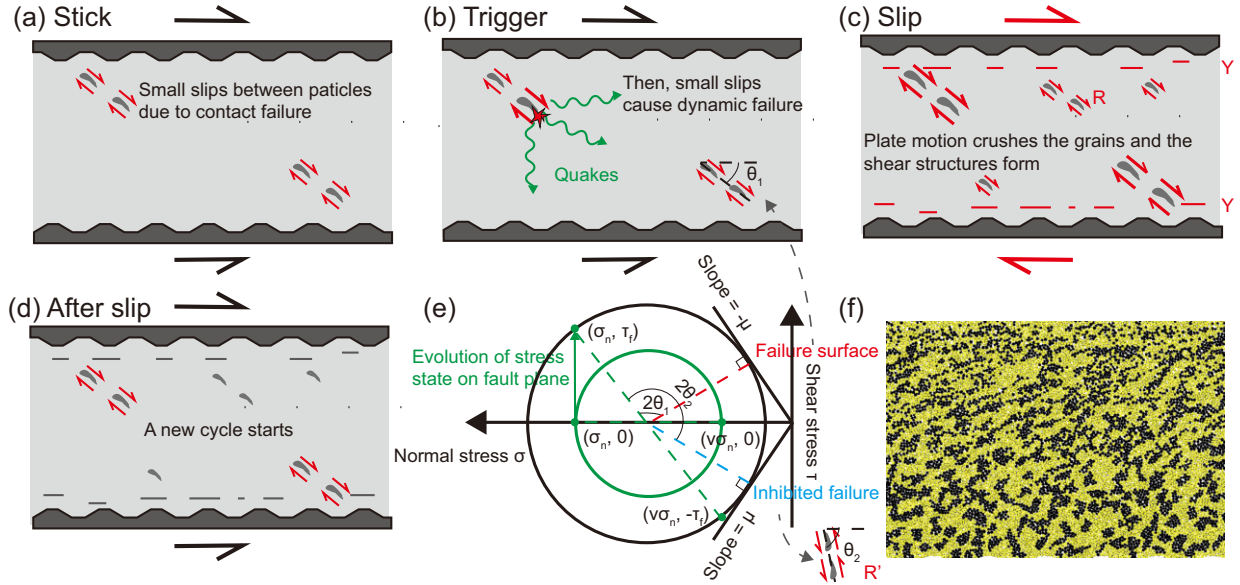


**Figure 8.** Formation mechanism of shear structures. (a)–(d) show the formation of shear structures. Red lines indicate relative slips between particles. Deep grey colour textures indicate the formed shear structures. (e) presents the Mohr–Coulomb circle to illustrate the angle of R shear, where  $\mu$  is the friction coefficient between particles,  $\sigma_n$  is the applied normal stress on faults,  $\tau_f$  is the corresponding shear stress where the faults transverse from stick phase to slip phase and  $\nu$  is the Poisson’s ratio of the granular gouge. The green circle indicates the stress state after consolidation. The black circle indicates the stress state when slip events occur and the green dashed line is the stress state on the fault plane at this moment. The two black lines tangent to the circle are the Mohr–Coulomb envelope of the granular mass, and the tangent points are the positions of the possible two failure surfaces. (f) shows the breakage of grains in the area we focus on in the stick-slip stage.

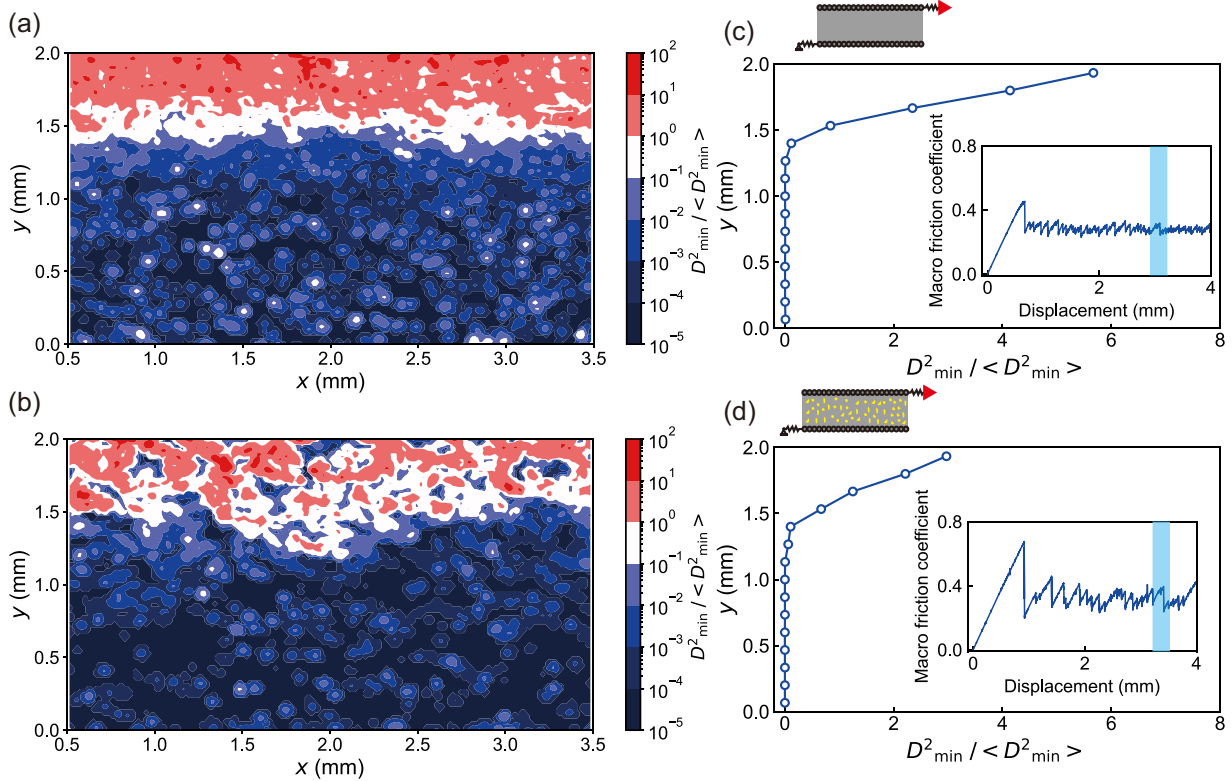


**Figure 9.** Granular plasticity in models without bonds and with unbreakable bonds. (a) The cloud map of non-affine displacement for the model without bonds, and (b) for the model with unbreakable bonds. (c)–(d) are the corresponding average values of non-affine displacement along the  $y$ -axis for the two models shown in (a) and (b), respectively. We use an arithmetic sequence to divide the  $y$ -axis into 15 equal layers and calculate the average  $D^2_{min} / \langle D^2_{min} \rangle$  of particle for each layer. The insets in (c)–(d) show the evolution of the macroscopic friction coefficient, and the shaded rectangles mark the periods in which the non-affine displacement is accumulated for (a) and (b), respectively.

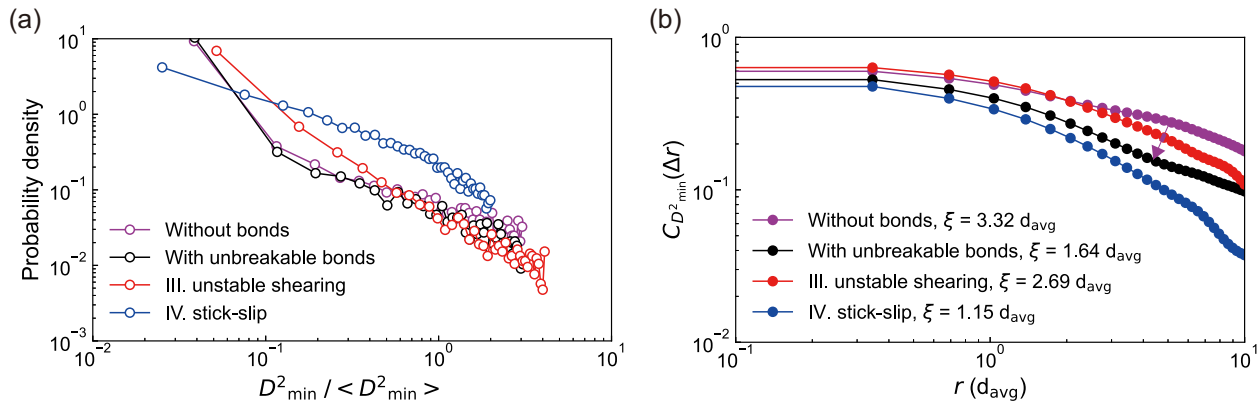


**Figure 10.** Distribution and correlation of plasticity in gouges without bonds and with unbreakable bonds. (a) Distribution of the normalized non-affine displacement. (b) Correlation of non-affine displacement. The corresponding results in the unstable shearing and stick-slip stages in the model with breakable grains are also plotted for comparison.

the grains can jam the gouge (Figs 9b and d). The plates tend to be locked, and the fault can store more elastic energy, thus producing much larger stress drops with longer stick durations. Notably, the shear localization zone in the two new extreme cases will not expand after longer shear displacement, and the breakage of grains in the model with breakable grains will expand the shear localization zone. Therefore, in the model with breakable grains, the shear localization decreases from unstable shearing to stick-slip, and so does the correlation.

Moreover, in the model with breakable grains, the plasticity tends to localize in the layer where the grains are broken because these particles are easier to flow in these places. The plates crush the grains during the stick-slip cycles, and in turn, the layer with finer grain size has a weaker ability to transmit the shear force. Thus, the formed structure influences the macroscopic property of faults and prohibits other grains from breaking. In our model, the particles cannot break again. However, in natural faults or laboratory earthquakes, due to the shear localization in these shear structures, the size of grains can get much finer in these places due to the accumulated plasticity, which strengthens the phenomenon and can be an explanation for fault lubrication and the existence of super fine gouge in principal slip zone (Han *et al.* 2010; Reches & Lockner 2010).

Pozzi *et al.* (2022) sheared granular gouges with different shear fabrics in the laboratory. The shear fabrics are pre-made by shearing the same gouge material under different normal stresses, and higher normal stresses result in much finer grains in the shear structure and correspond to more matured shear fabrics. The matured shear fabrics result in much larger friction drops in unstable shearing stages due to less weak grains and lower fault strength in the stick-slip stage due to fine gouge particles. In our work here, the model without bonds and with unbreakable bonds do not contain weak grains; they produce much larger friction drops in the unstable shearing stage than the model with breakable grains (Fig. 5b). The model without bonds and with breakable grains also corresponds to a lower fault strength in the stick-slip stage compared to the model with unbreakable bonds in which the rearrangement of the gouge is always jammed by grains (Figs 9c and d).

### 4.3 Implications and limitations

There are mainly three kinds of principal slip zone (PSZ) in existing laboratory earthquakes: (1) one PSZ right in the middle layer of the gouge (Ma *et al.* 2021; Zou *et al.* 2021), (2) one PSZ close

to the loading plate (Pozzi *et al.* 2021) and (3) two PSZs close to the two plates (Pozzi *et al.* 2023). The PSZ in the middle is because the particle size in their model is relatively large compared to the fault thickness, so the plates have extended influence ranges. The PSZ close to the loading plate is because the grains near the plate are easier to crush, and shear localizations in other places are inhibited. However, two PSZs close to the two plates will form in some circumstances. If the elastic rebound of the two plates is too drastic or the gouge is thick enough, two PSZs will form close to the two plates due to the decreased inhibition between the two PSZs. This also implies how fault structures form in natural faults. Taking the Zuccale fault core (Colletini *et al.* 2011) as an example (see in Fig. 11), the strong lens of carbonate is surrounded by the foliated and phyllosilicate-rich zone. These specific structures may be an evolutionary result of the long-term stick-slip cycles. Due to the phyllosilicate-rich zone being easier to flow and accommodate shear strain, the carbonate can maintain a block shape. There are fractures like R shear in the fault core, and a slip event may result from the reactivation of an existing R shear. However, this mechanism of the formation of shear structures is induced by our numerical simulations of laboratory experiments. With the improvement of 3-D geological modelling, simulations for the evolution of shear structures in real shear zones should be carried out for a more comprehensive study.

In our model, the breakage of irregular grain does render the gouge flow easier in the corresponding layer. However, when the granular gouge is only composed of large breakable spherical grains, the porosity of the granular gouge is high. Abe & Mair (2009) and Wang *et al.* (2021) found that the pores between spherical grains are filled with small particles in the shear process, which increase the friction strength of the fault system. In laboratory experiments, some researchers found that the shear localized in the layer with finer grain size (Scuderi *et al.* 2017; Pozzi *et al.* 2022; Pozzi *et al.* 2023), which is consistent with our work. However, when shearing granular gouge with higher porosity, some researchers found that the fine gouge particle will gradually saturate the porous shear zone (Chang *et al.* 2024a,b), and finer grain size did not mean shear will be localized in these places. Therefore, the results of our model correspond to the granular gouge with a low porosity.

Limited by the constitutive model, the unbonded particles are rigid discs and cannot break again. Although the simulated fault does show characteristics of the stick-slip cycle which is analogue to laboratory earthquakes and the Y shear band can be observed

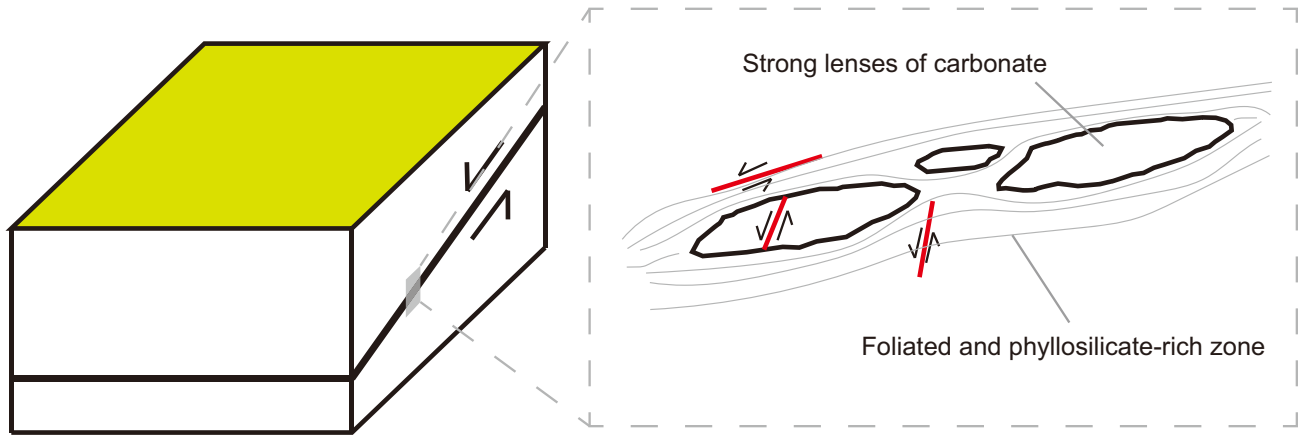


**Figure 11.** Typical shear structures in natural faults, taking the Zuccale fault core as an example (Collettini *et al.* 2011).

in the numerical model, we cannot find an obvious R shear band similar to that in the laboratory but just several isolate high granular temperature areas lined like R shear. A more refined numerical model that takes the damage of the mechanical property of a single particle into account may capture more realistic shear structures in the future. Also, the basic particles are rigid discs here, which decreases the interlock in the granular gouge (Zou *et al.* 2021). Therefore, the strength (macroscopic friction coefficient) of the simulated fault is lower than that of the real experiment (Scuderi *et al.* 2017; Pozzi *et al.* 2022). The basic particles' shapes matter and can be changed into irregular shapes to be composed of breakable grains for further exploration in the future.

3-D spherical breakable grains have been incorporated into the numerical model by the researchers (Abe & Mair 2005, 2009; Mair & Abe 2008; Ioannidi *et al.* 2024). Here, based on the 2-D images of quartz gouge, we construct irregular breakable grains in a 2-D numerical model of sheared granular gouge. Our model presents the general characteristics of the experiments, so the micro granular flow in our model is worth explaining the effects caused by the breakage of irregular grains. However, the 2-D model simplifies one dimension, which results in discrepancies between the 2-D and 3-D models. Frye & Marone (2002) designed laboratory experiments to compare the 2-D (shearing paralleled cylinder rods) and 3-D models (shearing spherical grains). They found that the shear strength of the 2-D model is less than that of the 3-D model because of the absence of out-of-plane contacts in the 2-D model. Here, in our 2-D model, the irregularity of the grain of one dimension is ignored. In the 3-D model, the 3-D irregular grain may have a stronger jam of the granular flow and cause stronger stress heterogeneity. With the development of high-resolution computer tomography equipment, we can construct irregular breakable grains in 3-D numerical sheared granular gouges for further exploration in the future.

## 5 CONCLUSIONS

In this paper, a new sheared granular gouge model setup that incorporates large irregular breakable grains and sheared with finite stiffness is proposed. The simulated fault evolves in four stages: (I) linear stage, (II) yield stage, (III) unstable shearing stage and (IV) stick-slip stage. Plasticity develops during the shear. The linear stage has the weakest correlation of plasticity. The plasticity has a clustering trend and spatial correlation increases in the yield stage. In the unstable shearing stage, the plasticity localizes near the plates, so the correlation is the strongest. However, with the breakage of the grains, the localization of the plasticity and the

spatial correlation decrease in the stick-slip stage. We also explore the local granular dynamics to illustrate how the shear structures form during the stick-slips in the stick-slip stage. In the stick phase, small slips occur between some particles. The small slips can activate the gouge and finally cause dynamic failures in the gouge. This procedure is responsible for the formation of R shear, which can also accelerate the plate to frictionate fiercely with its counterpart and form the Y shear.

Gouge layers with finer grain sizes become weaker to transmit shear force, and it is easier for such granular materials to rearrange themselves, making the shear localization in these layers more intense. In laboratory earthquakes or natural faults, the size of grains can get much finer due to the accumulated plasticity. Although granular materials have been proven to flow like fluid when subjected to external influences (Kou *et al.* 2017), the granular gouge ruptures similarly to a solid during stick-slip cycles.

## ACKNOWLEDGMENTS

This work is supported by the National Key Research and Development Program of China (No. 2022YFF0800601), the National Natural Science Foundation of China (42374070) and the China Scholarship Council (No. 202308440538). ZD carried out the simulation and drafted the manuscript. KG revised and polished the manuscript. JS provided access to the DEM code and comments for the simulations. JS would like to acknowledge the UK Engineering and Physical Sciences Research Council (EP/W031221/1).

## SUPPORTING INFORMATION

Supplementary data are available at [GJIRAS](https://www.gjournals.org) online.

Please note: Oxford University Press is not responsible for the content or functionality of any supporting materials supplied by the authors. Any queries (other than missing material) should be directed to the corresponding author for the paper.

## DATA AVAILABILITY

The original data output from PFC can be found at <https://zenodo.org/records/13299599>. Relevant PFC scripts run in PFC to carry out the simulation and Python codes for the calculation of granular quantities and visualization can be found at <https://github.com/xiaoDai4/Formation-and-evolution-of-shear-structures-in-sheared-granular-gouge>.

## REFERENCES

- Abe, S. & Mair, K., 2005. Grain fracture in 3D numerical simulations of granular shear, *Geophys. Res. Lett.*, **32**.
- Abe, S. & Mair, K., 2009. Effects of gouge fragment shape on fault friction: New 3D modelling results, *Geophys. Res. Lett.*, **36**.
- Aubry, J. *et al.* 2018. Frictional heating processes and energy budget during laboratory earthquakes, *Geophys. Res. Lett.*, **45**, 12 274–12 282.
- Bally, A.W., 1983. *Strike Slip Tectonics*. American Association of Petroleum Geologists.
- Ben-Zion, Y. & Sammis, C., 2009. Mechanics, structure and evolution of fault zones, *Pure appl. Geophys.*, **166**, 1533–1536.
- Billi, A., 2005. Grain size distribution and thickness of Breccia and gouge zones from thin (<1 m) strike-slip fault cores in limestone, *J. Struct. Geol.*, **27**, 1823–1837.
- Byerlee, J.D. & Brace, W.F., 1968. Stick slip stable sliding and earthquakes—effect of rock type pressure strain rate and stiffness, *J. geophys. Res.*, **73**, 6031–6037.
- Cao, Y. *et al.* 2018. Structural and topological nature of plasticity in sheared granular materials, *Nat. Commun.*, **9**, 2911.
- Casas, N., Mollon, G. & Daouadji, A., 2022. DEM analyses of cemented granular fault gouges at the onset of seismic sliding: peak strength, development of shear zones and kinematics, *Pure appl. Geophys.*, **179**, 679–707.
- Chang, C., Noda, H., Hamada, Y., Huang, C., Ma, T., Wang, G. & Yamaguchi, T., 2024a. Comminution-Induced Transient Frictional Behavior in Sheared Granular Halite, *Geophys. Res. Lett.*, **51**, e2024GL109645.
- Chang, C., Noda, H., Xu, Q., Huang, D. & Yamaguchi, T., 2024b. Slow-to-fast transition and shear localization in accelerating creep of clayey soil, *Geophys. Res. Lett.* **51**, doi: 10.1029/2024GL111839.
- Chikkadi, V. & Schall, P., 2012. Non-affine measures of particle displacements in sheared colloidal glasses, *Phys. Rev. E*, **85**.
- Collettini, C., Niemeijer, A., Viti, C., Smith, S.A.F. & Marone, C., 2011. Fault structure, frictional properties and mixed-mode fault slip behavior, *Earth planet. Sci. Lett.*, **311**, 316–327.
- Cundall, P.A. & Strack, O.D.L., 1979. A discrete numerical model for granular assemblies, *Geotechnique*, **29**, 47–65.
- da Cruz, F., Emam, S., Prochnow, M., Roux, J.-N. & Chevoir, F., 2005. Rheophysics of dense granular materials: Discrete simulation of plane shear flows, *Phys. Rev. E*, **72**, 021309.
- Davis, G.H., Bump, A.P., García, P.E. & Ahlgren, S.G., 2000. Conjugate Riedel deformation band shear zones, *J. Struct. Geol.*, **22**, 169–190.
- Di Toro, G. *et al.* 2011. Fault lubrication during earthquakes, *Nature*, **471**, 494–498.
- Dorostkar, O., Guyer, R.A., Johnson, P.A., Marone, C. & Carmeliet, J., 2017. On the role of fluids in stick-slip dynamics of saturated granular fault gouge using a coupled computational fluid dynamics-discrete element approach, *J. geophys. Res.: Solid Earth*, **122**, 3689–3700.
- Fei, J., Jie, Y., Sun, X. & Xiong, H., 2020. Physical interpretation of shear-rate behaviour of soils and geotechnical solution to the coefficient of start-up friction with low inertial number, *Sci. Rep.*, **10**, 12162.
- Ferdowsi, B., Griffa, M., Guyer, R.A., Johnson, P.A., Marone, C. & Carmeliet, J., 2013. Microslips as precursors of large slip events in the stick-slip dynamics of sheared granular layers: A discrete element model analysis, *Geophys. Res. Lett.*, **40**, 4194–4198.
- Ferdowsi, B., Griffa, M., Guyer, R.A., Johnson, P.A., Marone, C. & Carmeliet, J., 2014. Three-dimensional discrete element modeling of triggered slip in sheared granular media, *Phys. Rev. E Stat. Nonlin. Soft Matter Phys.*, **89**, 042204.
- Frye, K.M. & Marone, C., 2002. The effect of particle dimensionality on Granular friction in laboratory shear zones, *Geophys. Res. Lett.*, **29**, 22–1–22–4.
- Guo, Y. & Morgan, J.K., 2006. The frictional and micromechanical effects of grain comminution in fault gouge from distinct element simulations, *J. geophys. Res.: Solid Earth*, **111**. doi: 10.1029/2005JB004049.
- Guo, Y. & Morgan, J.K., 2007. Fault gouge evolution and its dependence on normal stress and rock strength—Results of discrete element simulations: Gouge zone properties, *J. geophys. Res.: Solid Earth*, **112**. doi: 10.1029/2006JB004524.
- Han, R., Hirose, T. & Shimamoto, T., 2010. Strong velocity weakening and powder lubrication of simulated carbonate faults at seismic slip rates, *J. geophys. Res.: Solid Earth*, **115**. doi: 10.1029/2008JB006136.
- Holt, R.M., Kjølås, J., Larsen, I., Li, L., Gotusso Pillitteri, A. & Sønstebo, E.F., 2005. Comparison between controlled laboratory experiments and discrete particle simulations of the mechanical behaviour of rock, *Int. J. Rock Mech. Min. Sci.*, **42**, 985–995.
- Ikari, M.J., Ito, Y., Ujiie, K. & Kopf, A.J., 2015. Spectrum of slip behaviour in Tohoku fault zone samples at plate tectonic slip rates, *Nat. Geosci.*, **8**, 870–874.
- Ioannidi, P.I., McLafferty, S., Reber, J.E., Morra, G. & Weatherley, D., 2024. Deformation and frictional failure of granular media in 3D analog and numerical experiments, *Pure appl. Geophys.*, **181**, 2083–2105.
- Itasca, 2021. *PFC—Particle Flow Code*, Ver. 7.0. Itasca, Minneapolis. <https://docs.itascacg.com/>
- Katz, Y., Weinberger, R. & Aydin, A., 2004. Geometry and kinematic evolution of Riedel shear structures, Capitol Reef National Park, Utah, *J. Struct. Geol.*, **26**, 491–501.
- Kimura, G. *et al.* 2022. Deformation process and mechanism of the frontal megathrust at the Nankai Subduction Zone, *Geochem. Geophys. Geosyst.*, **23**. doi: 10.1029/2021GC009855.
- Kou, B. *et al.* 2017. Granular materials flow like complex fluids, *Nature*, **551**, 360–363.
- Leeman, J.R., Saffer, D.M., Scuderi, M.M. & Marone, C., 2016. Laboratory observations of slow earthquakes and the spectrum of tectonic fault slip modes, *Nat. Commun.*, **7**, 11104.
- Li, Y., Hu, W., Xu, Q., Huang, R., Chang, C., Chen, J. & Wang, Y., 2024. Velocity profile geometries and granular temperature distributions in very dense granular flows, *Geophys. Res. Lett.*, **51**, e2023GL104410.
- Ma, G., Zou, Y., Chen, Y., Tang, L., Ng, T.-t. & Zhou, W., 2021. Spatial correlation and temporal evolution of plastic heterogeneity in sheared granular materials, *Powder Technol.*, **378**, 263–273.
- Mair, K. & Abe, S., 2008. 3D numerical simulations of fault gouge evolution during shear: Grain size reduction and strain localization, *Earth planet. Sci. Lett.*, **274**, 72–81.
- Mair, K. & Marone, C., 1999. Friction of simulated fault gouge for a wide range of velocities and normal stresses, *J. geophys. Res.: Solid Earth*, **104**, 28 899–28 914.
- Marone, C., 1998. Laboratory-derived friction laws and their application to seismic faulting, *Annu. Rev. Earth Planet. Sci.*, **26**, 643–696.
- Mei, J., Ma, G., Tang, L., Gao, K., Cao, W. & Zhou, W., 2023. Spatial clustering of microscopic dynamics governs the slip avalanche of sheared granular materials, *Int. J. Plast.*, **163**, 103570.
- Mora, P. & Place, D., 1999. The weakness of earthquake faults, *Geophys. Res. Lett.*, **26**, 123–126.
- Morgan, J.K., 1999. Numerical simulations of granular shear zones using the distinct element method: 2. Effects of particle size distribution and interparticle friction on mechanical behavior, *J. geophys. Res.: Solid Earth*, **104**, 2721–2732.
- Munjiza, A., 2004. *The Combined Finite-Discrete Element Method*. John Wiley & Son.
- Okubo, K., Bhat, H.S., Rougier, E., Marty, S., Schubnel, A., Lei, Z., Knight, E.E. & Klinger, Y., 2019. Dynamics, radiation, and overall energy budget of earthquake rupture with coseismic off-fault damage, *J. geophys. Res.: Solid Earth*, **124**, 11771–11801.
- Passelegue, F.X., Aubry, J., Nicolas, A., Fondriest, M., Deldicque, D., Schubnel, A. & Di Toro, G., 2019. From fault creep to slow and fast earthquakes in carbonates, *Geology*, **47**, 744–748.
- Place, D. & Mora, P., 2000. Numerical simulation of localisation phenomena in a fault zone, *Pure appl. Geophys.*, **157**, 1821–1845.
- Potyondy, D.O. & Cundall, P.A., 2004. A bonded-particle model for rock, *Int. J. Rock Mech. Min. Sci.*, **41**, 1329–1364.

- Pozzi, G., Collettini, C., Scuderi, M.M., Tesi, T., Marone, C., Amodio, A. & Cocco, M., 2023. Fabric controls fault stability in serpentinite gouges, *Geophys. J. Int.*, **235**, 1778–1797.
- Pozzi, G., De Paola, N., Nielsen, S.B., Holdsworth, R.E., Tesi, T., Thieme, M. & Demouchy, S., 2021. Coseismic fault lubrication by viscous deformation, *Nat. Geosci.*, **14**, 437–442.
- Pozzi, G., Scuderi, M.M., Tinti, E., Nazzari, M. & Collettini, C., 2022. The role of fault rock fabric in the dynamics of laboratory faults, *J. geophys. Res.: Solid Earth*, **127**.
- Reches, Z. & Lockner, D.A., 2010. Fault weakening and earthquake instability by powder lubrication, *Nature*, **467**, 452–455.
- Sammis, C., King, G. & Biegel, R., 1987. The kinematics of gouge deformation, *Pure appl. Geophys.*, **125**, 777–812.
- Scuderi, M.M., Collettini, C., Viti, C., Tinti, E. & Marone, C., 2017. Evolution of shear fabric in granular fault gouge from stable sliding to stick slip and implications for fault slip mode, *Geology*, **45**, 731.
- Villeneuve, M.C., Diederichs, M.S. & Kaiser, P.K., 2012. Effects of Grain Scale Heterogeneity on Rock Strength and the Chipping Process, *Int. J. Geomech.*, **12**, 632–647.
- Wang, D., Carmeliet, J., Zhou, W. & Dorostkar, O., 2021. On the effect of grain fragmentation on frictional instabilities in faults with granular gouge, *J. geophys. Res.: Solid Earth*, **126**. doi: 10.1029/2020JB020510.
- Yu, 2004. Discrete element method, *Eng. Comput.*, **21**, 205–214.
- Zou, Y., Ma, G., Mei, J., Zhao, J. & Zhou, W., 2021. Microscopic origin of shape-dependent shear strength of granular materials: A granular dynamics perspective, *Acta Geotech.*, **17**, 2697–2710.